

Chapter 2

System Analysis

2.1 Introduction

Two of the fundamental questions in the design of impulse-based UWB systems, or simply UWB systems as referred to in this book, are how much transmitting power is needed and what resolution is required to distinguish different targets. For UWB applications involving targets of multiple stratified media, another important question likely to be raised is how the radiated electromagnetic (EM) wave or signal propagates in the stratified media and what effect reflections have on received signals. In this chapter, a system analysis is conducted to find answers for these problems for the design of UWB systems. For illustration purposes, the analysis assumes a multi-layer structure as a specific target to be sensed by a UWB system. The analysis results will be used as reference specifications for the design of a UWB system to be described in subsequent chapters including transmitter, receiver, and antenna.

Specifically, the purposes of the system analysis performed here are to make rough estimations of the required power budget (i.e., required transmitting power) and range resolution for UWB systems. This simple analysis avoids the need of delving deeply into more complicated analysis and design of UWB systems which require more accurate information for the targets and more sophisticated modeling of the transmission and reflection of EM waves in multi-layer structures. More general and in-depth analysis of UWB systems can be found in the literature. The power budget analysis is based on the method of factorization of total loss presented in [1]. The resolution is determined predominantly by the radiating pulse duration, and hence an estimation of the required minimum pulse duration is derived based on the minimum thickness among the layers of a multi-layer structure.

2.2 UWB System Operation

As mentioned in Chap. 1, there are various applications for UWB systems and hence there exist different operations for UWB systems. Herein, for illustration purposes, we consider a specific application of sensing a target represented by a stratified structure

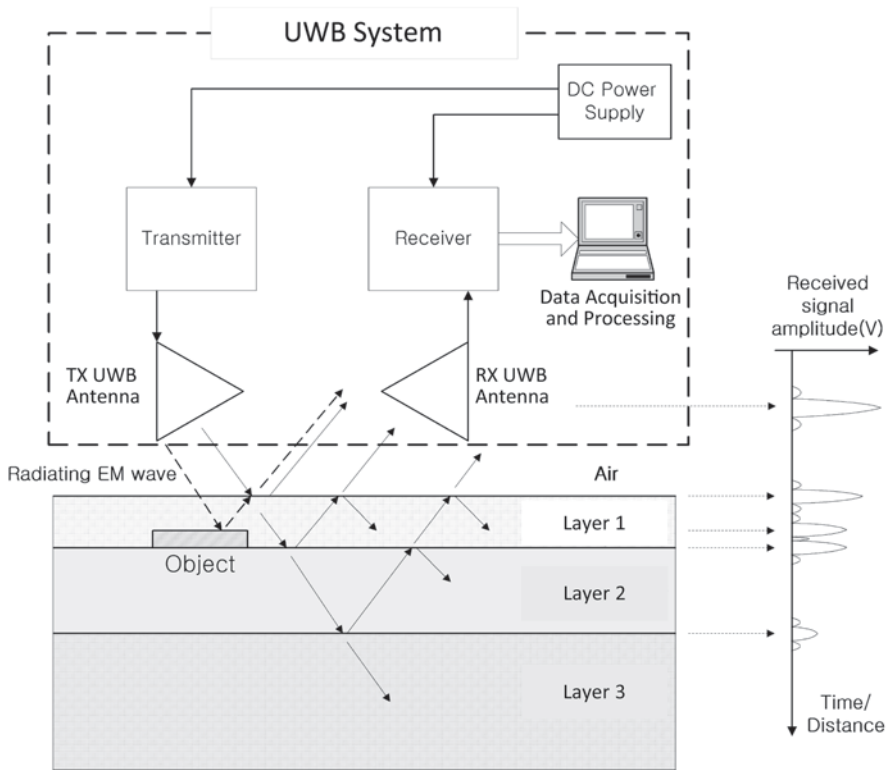


Fig. 2.1 UWB system and its operating principle in sensing the internal structure of a stratified-medium target

containing an object. Figure 2.1 shows a bistatic UWB system having separate transmitting and receiving antennas and its operational principle for this specific target. The UWB system is used to detect reflected signals from each interface between layers and the object. The first upper interface in Fig. 2.1 is formed between air and the first layer, and the second interface is formed between the first layer and the upper surface of the object, etc. The UWB system consists of a transmitter, a receiver, antennas, and a data acquisition and processing unit, similar to other sensing systems.

In Fig. 2.1, an EM pulse radiated from the transmitting antenna impinges on the surface of the target. Part of the incident wave to the surface is reflected back and captured by the receiving antenna. The remaining is transmitted into the first layer. This kind of reflection and transmission occurs on every layer interfaces as described in Fig. 2.1, and some of the reflected waves from each interface are captured by the receiving antenna. The received signal from the receiving antenna can be represented in the time domain as shown on the right-hand side of Fig. 2.1. Using this kind of received signals, we may identify the relative location of each interface and, eventually, the internal structure of the target. Further signal processing such as image processing can give more detection information for the layers and the object embedded within the target.

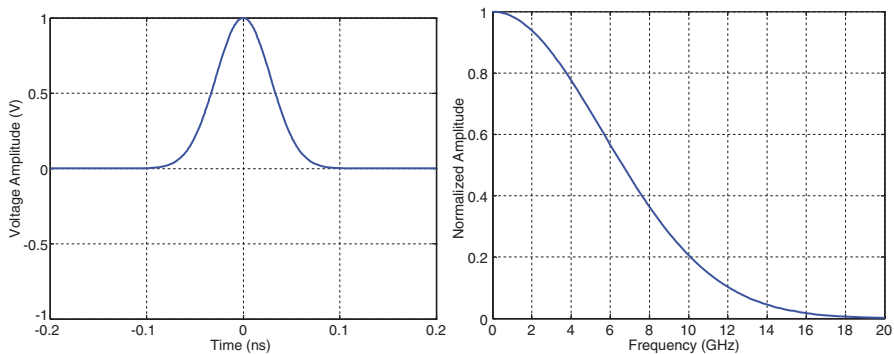


Fig. 2.2 Gaussian impulse with 200-ps pulse duration and its frequency spectrum

2.3 UWB Signals

The selection of impulse-signal types for UWB systems is one of the fundamental considerations in designing UWB systems, antennas, and circuits because the type of an impulse determines the UWB signal's spectrum characteristic. Many types of impulse signals such as step pulse, Gaussian-like (or monopolar) impulse, Gaussian-like single-cycle (or monocycle) pulse, Gaussian-like doublet pulse, and multi-cycle pulse can be used for UWB systems. Among those, Gaussian-like impulse, doublet pulse, and monocycle pulse are typically used in UWB systems. Particularly, the monocycle pulse is preferred in most UWB systems because of its spectral characteristics that facilitate easier wireless transmission than the impulse, wider bandwidth than the multi-cycle pulse, and easier to realize than the doublet pulse.

2.3.1 Gaussian Impulse

Figure 2.2 shows the time-domain waveform of a Gaussian impulse that has a shape of the Gaussian distribution, along with its frequency-domain waveform or spectral response. The impulse is assumed to have 200-ps pulse duration (or pulse width). The Gaussian impulse can be expressed as

$$y(t) = Ae^{-a^2t^2} \quad (2.1)$$

where A is the maximum amplitude of the Gaussian impulse and a is the constant that determines the slope of the Gaussian pulse. The spectral response containing the spectral components of the Gaussian impulse is obtained by taking its Fourier transform as

$$Y(\omega) = \frac{A}{a\sqrt{2}} e^{\frac{\omega^2}{4a^2}} \quad (2.2)$$

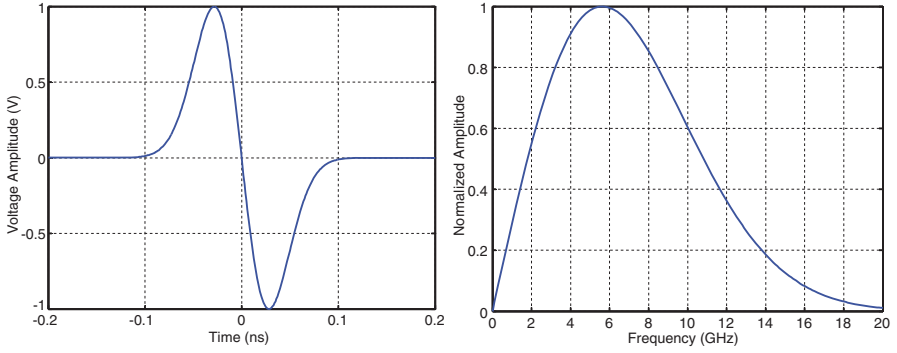


Fig. 2.3 Gaussian monocycle pulse with 200-ps pulse duration and its frequency spectrum

The frequency corresponding to the peak value of the impulse in the frequency domain is $f_o = 0$. The 3-dB bandwidth of the Gaussian impulse can be derived by letting the amplitude of the impulse at the 3-dB band-edge equal to the $1/\sqrt{2}$ of the maximum value at $f = 0$ as

$$\Delta f = 0.8326 \frac{a\sqrt{2}}{2\pi} \quad (2.3)$$

2.3.2 Gaussian Monocycle Pulse

Gaussian monocycle pulse is the first derivative of the Gaussian impulse signal. Figure 2.3 shows a Gaussian monocycle pulse having the same 200-ps pulse duration as the Gaussian impulse shown in Fig. 2.2 and its spectrum. The Gaussian monocycle pulse is described by

$$y(t) = -a^2 A t e^{-a^2 t^2} \quad (2.4)$$

The spectral response of the Gaussian monocycle pulse is given as

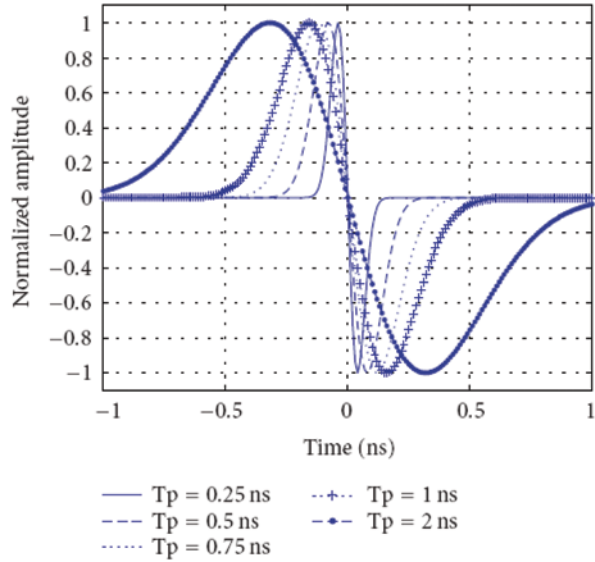
$$Y(\omega) = \frac{i\omega A}{a\sqrt{2}} e^{-\frac{\omega^2}{4a^2}} \quad (2.5)$$

The frequency corresponding with the peak value of the Gaussian monocycle pulse in the spectrum is obtained as

$$\Delta f_o = \frac{a\sqrt{2}}{2\pi} \quad (2.6)$$

and the 3-dB bandwidth can be derived as

Fig. 2.4 Gaussian monocycle pulses with different pulse durations



$$\Delta f = 1.155 \frac{a\sqrt{2}}{2\pi} = 1.155 f_o = \frac{1.155}{T_p} \quad (2.7)$$

where $T_p = 1/f_o$ is the pulse duration, which shows that the 3-dB bandwidth of the Gaussian monocycle pulse is approximately equal to 115 % of the pulse's center frequency f_o . Figs. 2.4 and 2.5 show the waveforms and spectrums of various Gaussian monocycle pulses having different pulse durations.

2.3.3 Gaussian Doublet Pulse

Figure 2.6 shows a Gaussian doublet pulse having 200-ps pulse duration and its spectrum. The Gaussian doublet pulse is the second derivative of the Gaussian impulse signal and hence can be expressed as

$$y(t) = -2a^2 A^{-a^2 t^2} (1 - 2a^2 t^2) \quad (2.8)$$

The spectral response of the Gaussian doublet pulse is

$$Y(\omega) = \frac{-A\omega^2}{a\sqrt{2}} e^{\frac{\omega^2}{4a^2}} \quad (2.9)$$

The frequency at which the peak value of the Gaussian doublet pulse occurs in the spectrum is

Fig. 2.5 Spectrum of Gaussian monocycle pulses with different pulse durations

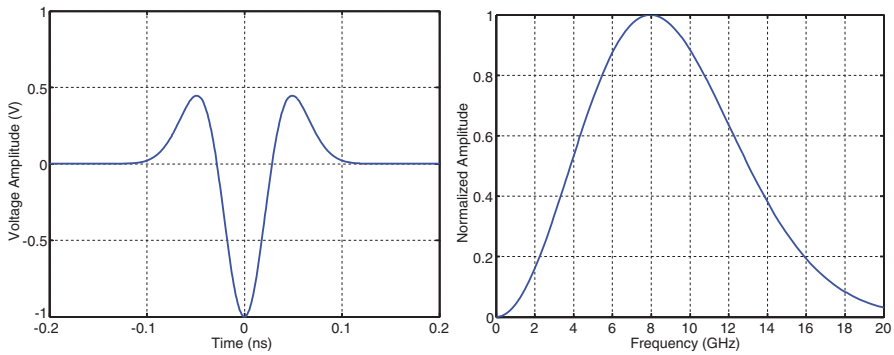
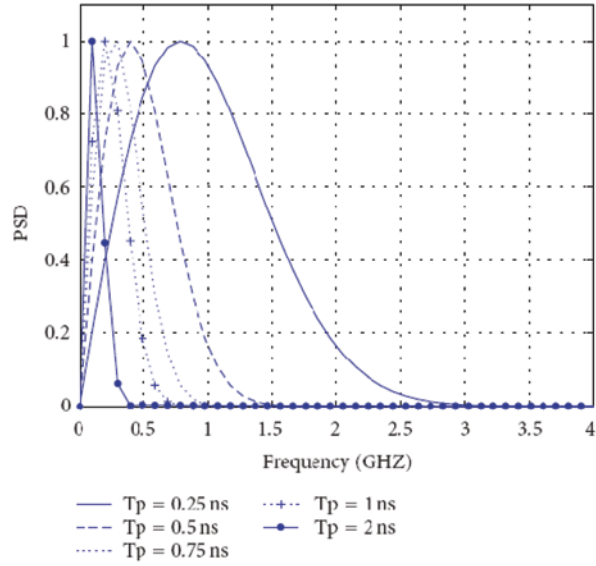


Fig. 2.6 Gaussian doublet pulse with 200-ps pulse duration and its frequency spectrum

$$f_o = \frac{a}{\pi} \quad (2.10)$$

This frequency is higher than that given in (2.6) for the Gaussian monocycle pulse. The 3-dB bandwidth can be derived as

$$\Delta f = 1.155 \frac{a\sqrt{2}}{2\pi} = 1.155 \frac{f_o}{\sqrt{2}} \quad (2.11)$$

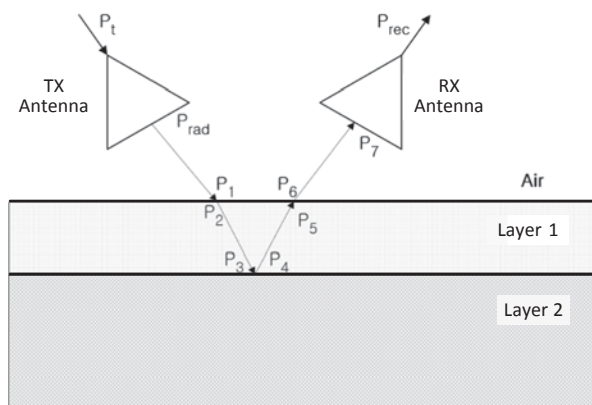
Compared to the bandwidth of the Gaussian monocycle pulse given in (2.7), the absolute bandwidth of the Gaussian doublet pulse is same, yet the fractional bandwidth

is larger assuming the same pulse duration. This result is due to the second-derivative performed upon the Gaussian impulse. Additional derivatives taken on the Gaussian impulse would produce other pulses having the same pulse duration but with progressively increasing fractional bandwidth and frequency corresponding to the peak pulse-magnitude. This phenomenon further implies that UWB signals generated using higher derivatives of the Gaussian impulse may be attractive for high-frequency UWB systems since they have higher frequencies and larger fractional bandwidth for the same pulse duration, which may be useful for some applications. It is noted that using a Gaussian monocycle pulse, which is the first derivative of a Gaussian impulse, at high frequencies requires a very narrow pulse duration which may be difficult to realize with sufficient amplitude in practice.

As can be seen from the pulse waveforms, the Gaussian impulse has no zero crossing point, while the Gaussian monocycle pulse and Gaussian doublet pulse have one and two zero crossings, respectively, which help define the bandwidth characteristics of these pulses. It is also observed that the spectral responses of these pulses contain no side-lobes beyond the zero-crossing frequency points which are desirable for signal transmission. For pulses whose spectral responses have side-lobes, such as a rectangular or sinusoidal pulse, these side-lobes are always outside the pass-band, which at most extends across the zero-crossing frequency ends, and hence produce unwanted radiation, leading to possible false-target detection and/or interference to other existing systems, especially when they have sufficiently high energy.

It is particularly noted that, as the peak spectral amplitude of the Gaussian impulse occurs at DC and as seen in Fig. 2.2, the bulk of its energy is contained at DC and low frequencies near DC. The monocycle and doublet pulse signals, on the other hand, contain no DC component and have much lower low-frequency energy. In general, the monocycle and doublet pulses have similar energy distributions in the low- and high-frequency regions around the center frequency. It is the difference in the spectral shapes of these signals at DC and low frequencies that greatly affects the transmission of signals via antennas and the propagation of signals through components, and ultimately the design of UWB antennas, components and systems. Impulses are not transmitted and received effectively through practical antennas due to their large portion of low-frequency spectral components which cannot be transmitted (or is transmitted with very low efficiency) by practical antennas. Monocycle and doublet pulses, on the other hand, can be transmitted more efficiently due to no DC component and less low-frequency content. Furthermore, using monocycle or doublet pulse facilitates the design of components including antenna in UWB systems due to no design consideration at DC and less design emphasis at low frequencies, leading to simpler and more compact design. It is further noted that signal fidelity is of utmost important for UWB systems which require signals to be transmitted and received with minimum distortion. With no DC component and less low-frequency spectral amplitudes contained in monocycle pulses, antennas and other system components can be more conveniently designed to cover desired bandwidth, hence minimizing the distortion of signals traveling through these components and, consequently, producing better fidelity for transmitting and receiving signals.

Fig. 2.7 Simplified diagram of incident and reflected signals on a two-layer object



UWB systems always transmit a train of pulses (typically periodically) instead of a single pulse. Consequently, according to Fourier analysis, the spectrums of UWB pulse signals are not continuous and contain discrete spectral lines (corresponding to discrete frequencies) spaced apart by $1/T$, where T is the period of the UWB signals. Fourier analysis also shows that a UWB signal consisting of a train of pulses is not substantially distorted by passive components including antennas having a bandwidth approximately equal to the reciprocal of the pulse width, because of most of the energy is contained within such bandwidth. According to the Parseval's theorem, the average power in a periodic pulse train is equal to the sum of the powers in its spectral components including DC and harmonics. Therefore, transmission of a UWB signal consisting of periodic high-voltage pulses would be similar to simultaneous transmission of strong CW signals at different frequencies. The results of the Parseval's theorem also suggest an alternate way of generating a UWB signal of periodic pulses by combining various CW signals having appropriate amplitudes and frequencies.

2.4 Power Budget Analysis

The power budget analysis involves estimating the minimum required transmitter output power to produce detectable reflected signals from a target. To illustrate this analysis, we consider a target consisting of two dielectric layers as shown in Fig. 2.7 together with the incident and reflected signals transmitted and received by the transmitter (TX) and receiver (RX) antennas of a system, respectively. For simplicity without loss of generality, we only consider the signal reflected from the second interface. That is, we are only interested in determining the power budget involved with the first layer and neglect the signals entering and reflected from the second layer 2. The analysis can be easily extended for multiple layers.

In Fig. 2.7, the signals transmitted and received by the transmitter and receiver, respectively, is represented by a power flow diagram that consists of the following

powers: P_t (transmitter's output power), P_{rad} (radiating power from the transmitting antenna), P_1 (incident power from air to interface 1 or air/layer 1 interface), P_2 (transmitting power from interface 1 into layer 1), P_3 (incident power from layer 1 to interface 2 or layer 1/layer 2 interface), P_4 (reflected power at interface 2), P_5 (incident power from layer 2 to interface 1), P_6 (transmitting power from interface 1 to air), P_7 (incident power from air into the receiving antenna), and P_{rec} (received power from the receiving antenna).

The received power P_{rec} in dBm can be expressed as

$$P_{rec} (dBm) = P_t + L_t \quad (2.12)$$

where L_t is the total loss defined as

$$L_t \equiv \frac{P_{rec}}{P_t} \quad (2.13)$$

The receiver sensitivity, S_i , in dB can be represented, using the required minimum transmitter's output power, $P_{t,min}$, as

$$S_i (dB) = P_{t,min} + L_t \quad (2.14)$$

which shows that the required minimum transmitter output power can be determined from the total loss and the receiver sensitivity determined by the receiver performance. For a given receiver, the main problem to determine $P_{t,min}$ is the calculation of the total loss. The total loss can be expressed using the powers defined in Fig. 2.7 as

$$L_t = \frac{P_{rec}}{P_7} \frac{P_7}{P_6} \frac{P_6}{P_5} \frac{P_5}{P_4} \frac{P_4}{P_3} \frac{P_3}{P_2} \frac{P_2}{P_1} \frac{P_1}{P_{rad}} \frac{P_{rad}}{P_t} \quad (2.15)$$

The power ratios in (2.15) can be grouped into several loss factors according to the cause of the loss [1]. We specify these loss factors as the antenna loss (L_{ant}), spreading loss (L_s), material attenuation loss (L_a), transmission coupling loss (L_{t1}), retransmission coupling loss (L_{t2}), and target scattering loss (L_{sc}). These loss factors are described as

$$L_{ant} = \frac{P_{rec}}{P_7} \frac{P_{rad}}{P_t} \quad (2.16)$$

$$L_s L_a = \frac{P_1}{P_{rad}} \frac{P_3}{P_2} \frac{P_5}{P_4} \frac{P_7}{P_6} \quad (2.17)$$

$$L_{t1} = \frac{P_2}{P_1} \quad (2.18)$$

$$L_{t2} = \frac{P_6}{P_5} \quad (2.19)$$

$$L_{sc} = \frac{P_4}{P_3} \quad (2.20)$$

It is noted that the antenna loss (L_{ant}) represents the total loss incurred by both transmitting and receiving antennas. The loss of each antenna can be divided further into the antenna efficiency (L_e) and the antenna mismatch loss (L_m). For instance, the antenna loss due to the transmitting antenna can be represented as

$$\frac{P_{rad}}{P_t} = \left(\frac{P_{rad}}{P_a} \right) \left(\frac{P_a}{P_t} \right) = L_e L_m \quad (2.21)$$

where P_a is the actual power entering the antenna. Using these definitions for loss factors, the total loss, L_t , in dB can be represented in terms of loss factors as

$$L_t (dB) = 2 L_e + 2 L_m + L_s + L_a + L_{t1} + L_{t2} + L_{sc} \quad (2.22)$$

In order to calculate the total loss, a detailed model for each loss factor is needed. The antenna efficiency (L_e) and mismatch loss (L_m) can be assumed simply as -1 dB which is reasonable for well-designed antennas. The other loss factors are elaborated as follows.

Spreading Loss (L_s) Spreading loss occurs due to reduction of the power density of a wave with distance as it propagates. The following well-known radar equation represents the spreading loss in a general form for bistatic systems:

$$\frac{P_{ra}}{P_{ta}} = \frac{A_{et} A_{er} \sigma}{4\pi R^4 \lambda^2} \quad (2.23)$$

where P_{ra} is the power received at the receiving antenna, P_{ta} is the power radiated from the transmitting antenna, A_{et} and A_{er} represent the effective apertures of the transmitting and receiving antennas, respectively, σ is the RCS (Radar Cross Section) of the target, R is the range from the system to the target, and λ is the operating wave length. The RCS is not considered in the spreading loss here; it will be dealt with in the target scattering loss later. After factoring out the RCS term, (2.23) can be simplified as

$$L_s = \frac{G_t A_{er}}{(4\pi R^2)^2} \quad (2.24)$$

where G_t is the transmitting antenna gain. Equation (2.24) indicates that the spreading loss is a function of the inversed 4th power of the range. This relationship with the range is reasonable only for a point reflector type target. However, in the case of a planar reflector type such as ground interface, the spreading loss expression needs to be modified and can be approximated as

$$L_s = \left. \frac{P_r}{P_{rad}} \right|_{L_a=0dB} \cong \frac{G_t A_{er}}{(4\pi)^{3/2} R^2} = \frac{G^2 \lambda^2}{(4\pi)^{5/2} R^2} \quad (2.25)$$

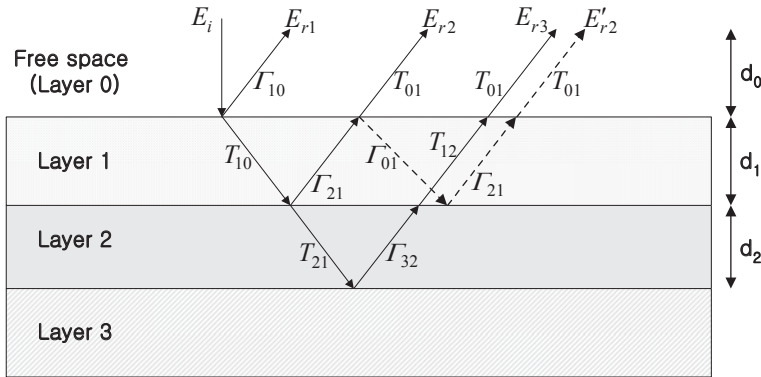


Fig. 2.8 Main reflections and transmissions in multi-layer structure

where G is the antenna gain assuming identical transmitting and receiving antennas. L_s is expressed in terms of the powers P_7 and P_{rad} defined in Fig. 2.7. In (2.25), no material attenuation effect is involved and the wavelength λ is not a single value due to wave propagation in different media such as those depicted in Fig. 2.7.

Material Attenuation Loss (L_a) EM waves propagating in a (practical) lossy medium experiences loss or attenuation of its power. The attenuation constant α of a lossy material can be found in the expression for the complex propagation constant γ of lossy materials as

$$\gamma = \alpha + j\beta = j\omega\sqrt{\mu\epsilon'\left(1 - j\frac{\epsilon''}{\epsilon'}\right)} \quad (2.26)$$

where β is the phase constant, ϵ' and ϵ'' are the real and imaginary parts of the material's complex dielectric constant, μ is the permeability of the material, and ω is the radian frequency. The attenuation constant α of a material can be approximately obtained by an expansion of (2.26) as

$$\alpha = \omega\sqrt{\frac{\mu\epsilon'}{2}(\sqrt{1 + \tan^2 \delta} - 1)} \quad (2.27)$$

where $\tan\delta \equiv \epsilon''/\epsilon'$ is the loss tangent of the material. The total attenuation or loss in dB for waves propagating a distance R in a material is then expressed as

$$L_a(\text{dB}) = -8.686\omega R\sqrt{\frac{\mu\epsilon'}{2}(\sqrt{1 + \tan^2 \delta} - 1)} \quad (2.28)$$

Transmission Coupling Loss (L_{t1}), Retransmission Coupling Loss (L_{t2}), and Target Scattering Loss (L_{sc}) Transmission coupling loss (L_{t1}), retransmission coupling loss (L_{t2}), and target scattering loss (L_{sc}) are related to the reflection and transmission of EM waves at the interface of different media. Figure 2.8 shows a target

consisting of multiple layers of materials and a simplified reflection-transmission diagram illustrating multiple reflections and transmissions of electric fields (and hence waves) occurred in the layers.

In Fig. 2.8, for simple analysis, it is assumed that the radiated electric field from the transmit antenna impinges perpendicularly on the surface of the multi-layer structure. The reflections and transmissions for oblique incidence of waves with parallel or perpendicular polarization can be easily extended. In Fig. 2.8, E_i represents the incident electric field intensity onto the first interface; E_{rk} , where k is an integer, represents the returned electric field intensity caused by the (first) single reflection at the k th interface; E_{rk}' represents the returned electric field intensity caused by the (subsequent) double reflections at the k th interface, which is different from the reflection described by E_{rk} ; T_{mn} represents the transmission coefficient for the transmitted signal from the n th layer to m th layer; Γ_{mn} represents the reflection coefficient for the incident signal from the n th layer to m th layer. It is noted that the reflection-transmission diagram depicted in Fig. 2.8 is simplified to include only the main reflection-transmission pairs that significantly contribute to producing a detectable returned signal; it does not include all possible reflection and transmission pairs that would occur in multi-layer structures.

Using the reflection-transmission diagram in Fig. 2.3, we can obtain the expressions for the returned electric field intensities with respect to the incident field intensity, E_i , as

$$\frac{E_{r1}}{E_i} = \Gamma_{10} \quad (2.29)$$

$$\frac{E_{r2}}{E_i} = T_{10} \Gamma_{21} T_{01} \quad (2.30)$$

$$\frac{E_{r3}}{E_i} = T_{10} T_{21} \Gamma_{32} T_{12} T_{01} \quad (2.31)$$

$$\frac{E_{r2}'}{E_i} = T_{10} \Gamma_{21} \Gamma_{01} \Gamma_{21} T_{01} = T_{10} \Gamma_{21}^2 \Gamma_{01} T_{01} \quad (2.32)$$

It is noted that, the returned electric field intensity including double reflections at the 2nd interface, E_{r2}' , expressed in (2.32), is much smaller than others described in (2.29)–(2.31) because, in most sensing applications, the magnitude of the reflection coefficient is much smaller than that of the transmission coefficient and E_i . (2.32) includes three times more of reflections than others. Consequently, the resulting magnitude of (2.32) is much smaller than others and hence can be ignored. Equations (2.29)–(2.31) involving a single reflection can be written in general as

$$\frac{E_{rm}}{E_i} = \Gamma_{n,n-1} \prod_{m=1}^{n-1} (T_{m,m-1} T_{m-1,m}) \quad (2.33)$$

The reflection and the transmission coefficients in (2.33) can be calculated for normal incident waves as

$$\Gamma_{n,n-1} = \frac{\eta_n - \eta_{n-1}}{\eta_n + \eta_{n-1}} \quad (2.34)$$

$$T_{n,n-1} = \frac{2\eta_n}{\eta_n + \eta_{n-1}} \quad (2.35)$$

where $\eta_n = \sqrt{\mu/\epsilon_n}$ is the intrinsic impedance of the n th layer with μ and ϵ_n being the permeability and permittivity of the n th layer, respectively. The intrinsic impedance of lossy materials is complex; therefore, the reflection and transmission coefficients for lossy materials are also complex as well. To simplify the analysis, however, we assume low-loss materials and hence the intrinsic impedances can be assumed to be real.

The loss factors related to the reflection and transmission of signals are divided into two groups: one is L_{sc} relating to the reflection, and the other is L_{t1} and L_{t2} relating to the transmission. Since the reflected power from a target is related to the target's RCS as well as the reflection coefficient, the target scattering loss L_{sc} can be defined as [1]

$$L_{sc} = \frac{P_{ref}}{P_{inc}} = \sigma |\Gamma|^2 \quad (2.36)$$

or, in dB,

$$L_{sc} (dB) = 20 \log |\Gamma| + 10 \log \sigma \quad (2.37)$$

where P_{ref} is the reflected power, P_{inc} is the incident power, and σ is the RCS of the target. Since the RCS value of a dielectric half-space such as the ground is known as 1, it can be ignored in our analysis. The target scattering loss can therefore be approximated as a simple multiplication of all the reflection coefficients occurred at the interfaces on the signal propagation path. The transmission and retransmission coupling loss, L_{t1} and L_{t2} , are in general the multiplication of the transmission coefficients on two different propagation paths, one in a downward direction and the other in an upward direction, respectively. As a result, Eq. (2.33) turns out to be the total loss that includes all the loss factors related to the signal reflection and transmission effects on a single returned signal, E_m . This new total loss factor is defined as the transmission loss L_u :

$$L_u (dB) = L_{sc} + L_{t1} + L_{t2} = 20 \log \left| \frac{E_{rm}}{E_i} \right| \quad (2.38)$$

Required Minimum Transmitting Power

Calculations of the loss factors, according to the derived equations, require values of the physical and electrical parameters characterizing interested targets.

Table 2.1 Parameters of a typical pavement structure

Layer	Thickness range (inch)	Typical thickness (inch)
Asphalt	2–10	6
Base	4–14	10
Sub-base	N/A	8

Table 2.2 Electrical properties of a pavement structure. $\epsilon_r' = \epsilon_r$ and ϵ_r'' are the real and imaginary parts of the relative dielectric constant; α is the attenuation constant calculated from (2.27); and $\eta \equiv 120\pi/\sqrt{\epsilon_r}$ is the intrinsic impedance

Layer	ϵ_r'	ϵ_r''	α (Np/m) at 2 GHz	η (Ω)
Asphalt	5–7	0.03–0.05	0.22–0.47	142–168
Base	8–12	0.3–0.8	1.8–5.9	108–133
Sub-base	20	N/A	N/A	84

As an example, we list in Table 2.1 the physical parameters of a typical pavement structure consisting of (top) asphalt, base, and (bottom) sub-base with normal physical dimensions. Table 2.2 summarizes the electrical parameters or properties of each layer of the pavement structure.

The required minimum transmitting output power for the considered payment structure can now be calculated based on the parameters in Table 2.1 and 2.2. The transmitting output power should be sufficient to detect the most distant object which is the 3rd interface between the base and sub-base layers of the pavement structure in this example. Therefore, the calculation of the required output power should be based on the returned signal from the 3rd interface. Let us assume that the interested frequency is 2 GHz which is the center frequency of a transmitting monocycle pulse with 400-ps duration. The thickness of the asphalt and base layers, depicted as d_1 and d_2 in Fig. 2.8, is assumed as 6 and 10 in., respectively. The distance between the end of the antenna aperture and the top of the asphalt layer, depicted as d_0 in Fig. 2.8, is assumed to be 10 in.

First, the spreading loss L_s is calculated using (2.25). The same antenna is used for the transmitting and receiving antennas, and the antenna gain G is assumed to be 10 dB which is reasonable for well-designed antennas such as the microstrip quasi-horn antenna to be described in Chap. 5. The range R is 50 in., which is the sum of d_0 , d_1 and d_2 . The calculated L_s is -22.6 dB.

Second, the total material loss L_a is determined as the sum of the losses in all layers calculated using (2.28). Let L_{a1} and L_{a2} be the loss per unit length in dB/m for the asphalt (layer 1) and base (layer 2), respectively. These losses can be obtained as -8.686α , where α is the attenuation constant of the individual layer in Neper/m. Calculation results using the maximum values for α provided in Table 2.2 give $L_{a1} = -4.08$ dB/m and $L_{a2} = -51.2$ dB/m. The traveling distance in each layer is twice of its thickness ($2d_1 = 0.5$ m and $2d_2 = 0.7$ m). Therefore, the total material loss in dB is $L_a = 2L_{a1}d_1 + 2L_{a2}d_2 = -37.9$ dB.

Third, the transmission loss L_u defined as (2.38) is calculated. As mentioned earlier, we are interested in the detection of the farthest object which is the 3rd

interface, which necessitates the calculation of $L_u = 20 \log |E_{r3}/E_i|$ using (2.31). The reflection and the transmission coefficients included in (2.31) can be calculated using (2.34) and (2.35), respectively. The intrinsic impedances for the layers are obtained as $\eta_0 = 377 \Omega$, $\eta_1 = 150 \Omega$, $\eta_2 = 120 \Omega$, and $\eta_3 = 84 \Omega$ based on the electrical properties of these layers listed in Table 2.2. The transmission loss can now be calculated as $L_u = -17$ dB.

Finally, using the calculated loss factors, the total loss can be obtained as $L_t = 2(L_e + L_m) + L_s + L_a + L_u = -82$ dB, where the antenna efficiency L_e and antenna mismatch loss L_m are assumed as -1 dB.

To obtain the required minimum transmitter output power according to (2.14), we need to know the receiver sensitivity S_i besides the total loss. Assume 8-dB tangential sensitivity for the receiver, which is generally used for measurement systems [2], we can express the receiver sensitivity in dB as

$$S_i(\text{dB}) = kTBF + \text{SNR}_o = kTBF + 8 \quad (2.39)$$

where $k = 1.38 \times 10^{-23} \text{ JK}^{-1}$ is the Boltzmann's constant, T is the absolute temperature in Kelvin degree ($^{\circ}\text{K}$), B is the receiver's bandwidth, F is the receiver's noise figure, and SNR_o is the required output SNR (Signal-to-Noise Ratio), which is 8 dB for the 8-dB tangential sensitivity. The calculation result for the receiver sensitivity using $T = 298 \text{ }^{\circ}\text{K}$ (room temperature), $B = 5 \text{ GHz}$ and $F = 3 \text{ dB}$ is $S_i = -66$ dB. Using (2.14) and the calculation result for the total loss and sensitivity, the required minimum transmitter power is obtained as $P_{t, \min} = 16$ dBm. Note that this is the average power for the CW signal, which is at 2 GHz as considered here. For a UWB signal such as the monocycle pulse, we are interested in the pulse peak power or peak-to-peak voltage value (V_{pp}). The conversion result from the average power to the peak-to-peak voltage value is $4 V_{pp}$ for $50\text{-}\Omega$ load, which is the required minimum voltage of the transmitter output pulse and is equivalent to 80 mW of the peak power.

2.5 Range Resolution Analysis

The minimum range resolution for UWB systems is required only for the detection of the thinnest layer in a multi-layer target. In our considered example of the pavement structure, the thinnest layer is the asphalt layer. Let us assume that the minimum thickness of the asphalt we need to discern from the base layer is 1 in. Therefore, the objective of the resolution analysis is finding the minimum required pulse duration to achieve the required range resolution of 1 in. We can find the minimum required pulse duration T_p from the simple equation of $T_p = d_m/v_p$, where d_m is the minimum thickness of the asphalt layer and v_p is the phase velocity of the propagating wave at a certain frequency. For low-loss materials, $v_p \cong \omega/\beta$ for plane waves, where the phase constant β may be approximated for low-loss materials as

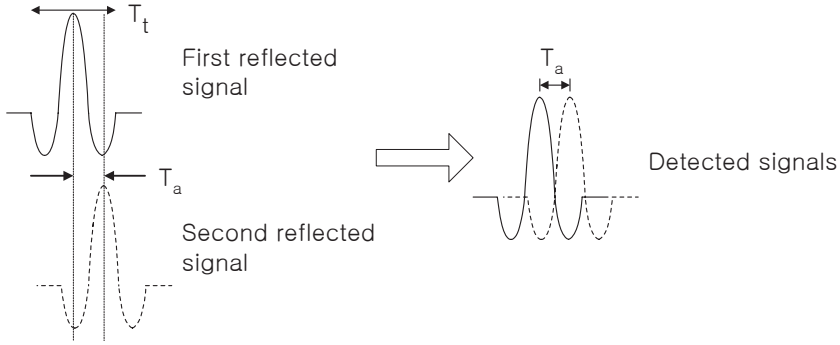


Fig. 2.9 Two detected signals with minimum discernable time interval

$$\beta \cong \omega \sqrt{\mu \epsilon'} \left(1 + \frac{1}{8} \tan^2 \delta \right) \cong \omega \sqrt{\mu \epsilon'} \quad (2.40)$$

where $\epsilon' = \epsilon_o \epsilon_r$ with ϵ_o being the permittivity of air. The phase velocity v_p can then be approximated for low-loss non-magnetic materials as

$$v_p \cong \frac{1}{\sqrt{\mu \epsilon'}} = \frac{1}{\sqrt{\mu_o \epsilon_o \epsilon_r}} = \frac{c}{\sqrt{\epsilon_r}} \quad (2.41)$$

where $c = 3 \times 10^8$ m/s. The phase velocity in the asphalt layer, whose relative dielectric constant is given in Table 2.2, is calculated from (2.41) as 4.46×10^9 to 5.28×10^9 in./sec. The minimum required pulse duration for the transmitting pulse is then determined as $T_p \cong 200$ ps. This short pulse duration, however, does not take into account the actual waveform shape in the detection stage. If the actual received waveform from the receiving antenna is considered, then the minimum pulse duration needed for the required range resolution is not the same as the transmitting pulse duration.

As we will use the microstrip quasi-horn antennas described in Chap. 5 for the UWB system presented in this book, let's assume TEM horn antenna is used for the transmitting and the receiving antennas in this analysis. For this type of antenna, the radiating signal is the first derivative of the input signal [3–5]. Therefore, for an input signal of monocycle pulse, the received waveform through the receiving antenna is approximately similar to the Sinc-function as seen in Fig. 2.9. Figure 2.9 shows two reflected signals from two different layer interfaces separated by a distance equal to the minimum range resolution, which are detected in sequence, generated from a monocycle pulse transmitted by a TEM horn antenna. The first and second reflected signals are from the first and second interfaces, respectively. The pulse duration T_t is assumed to be the same as that of the transmitting pulse, ignoring typically small pulse-stretching effect of a well-designed TEM horn antenna and other pulse effects due to the reflection coefficients at the interfaces. As shown in the waveforms of the

detected signals in Fig. 2.9, a minimum time interval T_a is required to completely discern the two detected signals without any overlap in the pulse main-lobes. In order to achieve that, T_a should be equal to the minimum required pulse duration, T_p . However, as shown in Fig 2.9, T_a is about a half of the transmitting pulse duration T_t . Therefore, the transmitting pulse duration T_t needed for achieving a range resolution of 1 in. is about twice the time of T_p , which is about 400-ps.

2.6 Summary

This chapter covers the theory and analysis of UWB systems, particularly the system operating principle, power budget and range resolution. Various UWB pulse signals commonly used for UWB systems, including Gaussian-like impulse, doublet pulse, and monocycle pulse, are addressed. Detailed calculations for the minimum required transmitting power and minimum required pulse duration for a specific range resolution are also presented using a typical multi-layer pavement structure.

References

1. Daniels, D.J.: Surface Penetrating Radar. IEE Press, London (1996)
2. Fontana, R.J., Richley, E.A., Beard, L.C., Barney, J.: A programmable ultra wideband signal generator for electromagnetic susceptibility testing. In 2003 IEEE Conference on Ultra Wideband Systems and Technologies, pp. 21–25 (2003)
3. Taylor, J.D.: Introduction to Ultra-Wideband Radar Systems. CRC Press: Boca Raton (1995)
4. Theodorou, E.A., Gorman, M.R., Rigg, P.R., Kong, F.N.: Broadband pulse-optimised antenna. IEE Proceedings, vol. 128, pt. H, no. 3, pp. 124–130 (June 1981)
5. Miao, M., Nguyen, C.: On the development of an integrated CMOS-based UWB tunable-pulse transmit module. IEEE Transactions on Microwave Theory and Technique, vol. MTT-54, No. 10, pp. 3681–3687 (October 2006)

Time-Domain Ultra-Wideband Radar, Sensor and
Components

Theory, Analysis and Design

Nguyen, C.; Han, J.

2014, VIII, 133 p. 95 illus., 42 illus. in color., Softcover

ISBN: 978-1-4614-9577-2